

BLACK HOLE FEEDBACK, GALAXY QUENCHING AND OUTFLOWS AT COSMIC DAWN: ANALYSIS OF THE SEEDZ SIMULATIONS

LEWIS R. PROLE^{* 1}, JOHN A. REGAN¹, DAXAL MEHTA¹, RÜDIGER PAKMOR², SOPHIE KOUDMANI^{7,11}, MARTIN A. BOURNE^{7,11}, SIMON C. O. GLOVER⁴, JOHN H. WISE⁵, RALF S. KLESSEN^{4,9}, MICHAEL TREMMEL⁶, DEBORA SIJACKI^{3,7}, RICARDA S. BECKMANN¹⁰, MARTIN G. HAEHNELT^{3,7}, JOHN BRENNAN¹, PELLE VAN DE BOR¹, AND PAUL C. CLARK⁸

¹ Centre for Astrophysics and Space Sciences Maynooth, Department of Physics, Maynooth University, Maynooth, Ireland.

² Max-Planck-Institut für Astrophysik, Karl-Schwarzschild-Straße 1, D-85748, Garching, Germany

³ Institute of Astronomy, University of Cambridge, Madingley Road, Cambridge CB3 0HA, UK

⁴ Universität Heidelberg, Zentrum für Astronomie, Institut für Theoretische Astrophysik, Albert-Ueberle-Straße 2, 69120 Heidelberg, Germany.

⁵ Center for Relativistic Astrophysics, School of Physics, Georgia Institute of Technology, 837 State Street, Atlanta, GA 30332, USA

⁶ School of Physics, University College Cork, College Road, Cork T12 K8AF, Ireland

⁷ Kavli Institute of Cosmology, Cambridge, University of Cambridge, Madingley Road, Cambridge CB3 0HA, UK

⁸ Cardiff University School of Physics and Astronomy

⁹ Universität Heidelberg, Interdisziplinäres Zentrum für Wissenschaftliches Rechnen, Im Neuenheimer Feld 225, 69120 Heidelberg, Germany

¹⁰ Institute for Astronomy, University of Edinburgh, Royal Observatory, Edinburgh EH9 3HJ, UK and

¹¹ Centre for Astrophysics Research, Department of Physics, Astronomy and Mathematics, University of Hertfordshire, College Lane, Hatfield, AL10 9AB, UK

Version February 11, 2026

ABSTRACT

Here we analyse the growth and feedback effects of massive black holes (MBHs) in the SEEDZ simulations. The most massive black holes grow to masses of $\sim 10^6 M_{\odot}$ by $z = 12.5$ during short bursts of super-Eddington accretion, sustained over periods of 5-30 Myr. We find that the determining factor that cuts off this initial growth is feedback from the MBH itself, rather than nearby supernovae or exhausting the available gas reservoir. Our simulations show that for the most actively accreting MBHs, feedback completely evacuates the gas from the host halo and ejects it into the inter-galactic medium. Despite implementing a relatively weak feedback model, the energy injected into the gas surrounding the MBH exceeds the binding energy of the halo. These results either indicate that MBH feedback in the early (Λ CDM) Universe is much weaker than previously assumed, or that at least some of the high redshift galaxies we currently observe with JWST formed via a two-step process, whereby a MBH initially quenches its host galaxy and later reconstitutes its baryonic reservoir, either through mergers with gas rich galaxies or from accretion from the cosmic web. Moreover, the maximum black hole masses that emerge in SEEDZ are effectively set by a combination of MBH feedback modelling and the binding potential of the host halo. Unless feedback is extremely ineffective at early times (for example if growth is merger dominated rather than accretion dominated or feedback is contained close to the MBH) then the maximum mass of black holes at redshift before 12.5 should not significantly exceed $10^6 M_{\odot}$.

1. INTRODUCTION

The discovery by JWST of a substantial population of massive black holes (MBHs) of mass $> 10^6 M_{\odot}$, existing within the first billion years of the Universe ($z \gtrsim 6$) (Larson et al. 2023; Maiolino et al. 2024; Juodžbalis et al. 2024; Kovács et al. 2024; Bogdán et al. 2024; Taylor et al. 2025) has challenged our understanding of compact object formation in the early Universe. Moreover, it is unclear how these black holes (BHs) grew from their initial seed masses by orders of magnitude within the allotted time frame. Current observations of MBHs now extend out to $z \sim 12.3$ (Ortiz et al. 2025) and galaxy observations out to $z \sim 14.4$ (Carniani et al. 2024; Naidu et al. 2026). At these extreme redshifts, our understanding of galaxies, their small-scale properties, and their embedded black holes has previously relied heavily on theoretical models. However, the growing body of JWST

observations now allows us to integrate theory and observational data from the early Universe. The SEEDZ simulation suite was designed to take advantage of this observational data, with the goal of understanding early galaxy and MBH evolution.

Did the first MBHs form from the remnants of the first Population III stars (so-called light seed black holes) and somehow sustain Eddington growth rates throughout their lives? Or did short bursts of super-Eddington growth quickly amplify their masses (e.g. Madau & Rees 2001; Milosavljević et al. 2009; Alvarez et al. 2009; Lupi et al. 2016; Smith et al. 2018; Shi et al. 2023, 2024; Gordon et al. 2024, 2025; Zana et al. 2025; Mehta et al. 2024)? Was the required mass growth reduced by forming with higher initial masses (heavy seeds) via a number of connected formation pathways (Regan & Volonteri 2024)? Heavy seed MBHs could be born from runaway collisions within a dense stellar cluster (Begelman & Rees 1978; Portegies Zwart et al. 2004; Reinoso et al. 2018,

*email: lewis.prole@mu.ie

2023; Rantala & Naab 2025) or within a BH cluster (Fragnione & Leigh 2018). Alternatively, heavy seeds may be born from the end points of super-massive stars (SMSs) or perhaps quasi-stars (QSSs) (Loeb & Rasio 1994; Lodato & Rice 2004; Begelman et al. 2006; Wise et al. 2008; Begelman et al. 2008; Regan & Haehnelt 2009; Mayer et al. 2010; Agarwal et al. 2012, 2014; Habouzit et al. 2016; Inayoshi et al. 2015; Ardaneh et al. 2018; Luo et al. 2018; Regan & Downes 2018; Visbal et al. 2014a,b; Latif et al. 2013; Regan et al. 2014; Becerra et al. 2015; Regan et al. 2017; Wise et al. 2019; Regan et al. 2020; Latif et al. 2021; Chiaki et al. 2023; Prole et al. 2024a,b; Cenc & Habouzit 2025). In this case, rapid accretion onto a protostar in excess of $\sim 10^{-2} M_{\odot} \text{ yr}^{-1}$ is required to drive the formation of a bloated supermassive star with zero age main sequence masses between 10^3 and $10^5 M_{\odot}$ (e.g. Umeda et al. 2016; Woods et al. 2017; Haemmerlé et al. 2018, 2021; Nandal et al. 2023). The eventual collapse of these objects after approximately 2 Myr is thought to result in the direct formation of a heavy seed MBH.

More exotically, it is conceivable that the seeds for the SMBH population formed earlier in cosmic history as primordial black holes, giving them more time to grow into SMBHs (Kashlinsky 2021; Liu et al. 2022; Dayal 2024; Prole et al. 2025; Ziparo et al. 2025; Zhang et al. 2025) with potential observable effects in the very first galaxies (e.g. Maiolino et al. 2025).

Irrespective of how these high redshift SMBHs formed, their current observed relationships with respect to their host galaxies show stark differences to established local Universe trends (Pacucci et al. 2023; Pacucci & Loeb 2024; Dattathri et al. 2025). Most notably, the local black hole-stellar mass ($M_{\text{BH}}\text{-}M_{\text{star}}$) relationship follows $M_{\text{BH}}/M_{\text{star}} \simeq 10^{-4}$ (e.g. Reines & Volonteri 2015), while high redshift observations produce relatively over-massive black holes with $M_{\text{BH}}/M_{\text{star}} \gtrsim 10^{-2}$ (e.g. Pacucci et al. 2023; Matthee et al. 2025) – an effect we observed in the first paper in this series (Prole et al. 2025). This suggests that the stellar component of galaxies builds up after the formation of a MBH seed, transitioning from the high-redshift trends to the local relation over time as the host galaxy matures. Alternatively, the observed over-massive black hole to stellar mass ratios have been suggested to arise due to observational selection biases and measurement uncertainties, allowing only the so-called ‘tip of the iceberg’ to be observed (Li et al. 2024).

The first suite of SEEDZ simulations (Prole et al. 2025) were designed to investigate black hole formation and growth within a Λ CDM context, modeling light and heavy seed black holes in fully 3D hydrodynamic cosmological simulations, performed with the moving mesh code AREPO2 (Springel 2010; Pakmor et al. 2016, 2023). The simulations utilize new models for Population III star formation, supernovae (SNe) explosions and the resulting formation of light seed black holes, metal enrichment and subsequent Population II star formation, heavy seed black hole formation, Eddington and super-Eddington accretion schemes as well as black hole feedback. In Prole et al. (2025), we presented 3 simulations suites, referred to as RAREPEAK, NORMAL1 and NORMAL2. We showed that a number of heavy seeds were able to grow from their initial seed masses of $\sim 10^4 M_{\odot}$

into the upper $10^5 M_{\odot}$ regime by $z = 15$, giving a number density of massive objects ($> 10^5 M_{\odot}$) of a few times $10^{-2} \text{ cMpc}^{-3} \text{ h}^{-1}$. The simulations have now advanced to $z = 12.5$, and at least 1 MBH per simulation has exceeded $10^6 M_{\odot}$. We now aim to find the physical mechanism that causes a growing SMBH to stop accreting, and hence dictates its final mass at $z = 12.5$.

The paper is structured as follows; §2 summarizes the numerical methods relevant to BH growth used in the SEEDZ simulations. In §3 we present our results for MBH growth, galaxy quenching and outflows. In §4, we discuss these results and give our conclusions. Appendix A provides further evidence for the conclusions made.

2. NUMERICAL METHOD

Here we will cover the aspects of the SEEDZ simulations relevant to BH growth: accretion, feedback, dynamical friction and BH mergers. For details on the formation of stars, SNe explosions and subsequent light seed BH formation, we refer to the initial SEEDZ paper (Prole et al. 2025).

2.1. Black Hole Accretion

Upon formation, BH particles are assigned an accretion radius R_{acc} set to 5 times the chosen minimum cell length, giving $R_{\text{acc}} = 0.62 \text{ ckpc h}^{-1}$ (for example, this is $\sim 45 \text{ pc}$ physical at $z = 20$). We model accretion onto BHs as Bondi-Hoyle-Lyttleton (Bondi 1952) accretion, following the formulation set out in Krumholz et al. (2004) and Krumholz et al. (2006). The Bondi radius is given by

$$R_{\text{Bondi}} = \frac{GM_{\text{BH}}}{v_{\infty}^2 + c_{\infty}^2}, \quad (1)$$

where v_{∞} is the mass-weighted speed of the gas within the accretion radius relative to the BH and c_{∞} is the sound speed in the region. The accretion rate onto the BH is then calculated using the Bondi formula as defined in Krumholz et al. (2004)

$$\dot{M}_{\text{Bondi}} = 4\pi\rho_{\infty}R_{\text{Bondi}}^2((1.12c_{\infty})^2 + v_{\infty}^2)^{1/2} \quad (2)$$

where ρ_{∞} is the weighted density for each cell inside the accretion radius, computed as described below.

As the Bondi radius scales with the square of the black hole mass, we do not always resolve the Bondi radius. For lower mass light seed black holes this becomes particularly challenging, hence we do not resolve the Bondi radius of these black holes in any of the simulations presented in this paper (see Mehta et al. 2026 for a discussion on this point). In order to account for this, we follow Krumholz et al. (2004) and define a kernel radius which accounts for the resolution of the simulation relative to the Bondi radius. The kernel radius, r_K , is computed as:

$$r_K = \begin{cases} \Delta x_{\min}/4 & R_{\text{Bondi}} < \Delta x_{\min}/4 \\ R_{\text{Bondi}} & \Delta x_{\min}/4 \leq R_{\text{Bondi}} \leq R_{\text{acc}}/2 \\ R_{\text{acc}}/2 & R_{\text{Bondi}} > R_{\text{acc}}/2 \end{cases} \quad (3)$$

where Δx_{\min} is the global minimum cell radius, estimated from the cell volume V as $(3V/4\pi)^{1/3}$. A Gaussian kernel radius is used to assign a weight to every cell within R_{acc} using

$$W \propto \exp(-r^2/r_K^2), \quad (4)$$

where r is the distance from the cell to the accreting BH. The weighted density ρ_∞ is then calculated as:

$$\rho_\infty = \bar{\rho}W \quad (5)$$

where $\bar{\rho}$ is the mass-weighted mean density within the accretion sphere.

2.1.1. Vorticity Adjustment

Following [Krumholz et al. \(2006\)](#) and [Mehta et al. \(2024\)](#), we further adjust the accretion rate based on the vorticity ω of the surrounding gas. Low angular momentum gas is preferentially much easier to accrete and accounting for the vorticity of the gas addresses over-accretion of high angular momentum gas. The vorticity of the gas is given by

$$\omega = |\nabla \times \vec{v}| \quad (6)$$

of which we take the mass weighted average within the accretion sphere. We then calculate the dimensionless vorticity ω_* as

$$\omega_* = \omega \frac{R_{\text{Bondi}}}{c_\infty}. \quad (7)$$

and introduce a damping factor $f(\omega)$ defined as

$$f_w = \frac{1}{1 + \omega_*^{0.9}}. \quad (8)$$

The accretion rate in a turbulent medium can then be calculated according to

$$\dot{M}_\omega = 4\pi\rho_\infty R_{\text{Bondi}}^2 c_\infty (0.34f_w). \quad (9)$$

The total accretion rate onto the BH particle is

$$\dot{M} = (\dot{M}_{\text{Bondi}}^{-2} + \dot{M}_\omega^{-2})^{-0.5}. \quad (10)$$

For a given time step, t_h , the mass of the BH particle increases by $M_{\text{acc}} = t_h \dot{M}$, which is removed from cells within R_{acc} using the weighting scheme calculated in Equation 4, adjusting the velocities of both the gas cells and the BH to conserve linear momentum. The BH position is then shifted to the center of mass of a system comprised of the BH and the accreted mass contributions from each cell.

2.2. Black Hole Accretion Feedback

To account for BH accretion feedback, we inject thermal energy into gas cells within the accretion region isotropically, based on the accretion rate onto a BH. The total mass accreted during a single timestep is given by M_{acc} . This produces an amount of thermal energy

$$E_{\text{th,acc}} = \epsilon f_c M_{\text{acc}} c^2, \quad (11)$$

where f_c is the thermal coupling factor, which we set to 0.05 (see e.g. [Booth & Schaye 2009](#)), and ϵ is the radiative efficiency. The calculation of ϵ changes based on whether the BH is accreting at sub- or super-Eddington rates. For sub-Eddington accretion rates, we calculate ϵ as

$$\epsilon = 1 - \sqrt{1 - \frac{2}{3R_{\text{ISCO}}}}, \quad (12)$$

where R_{ISCO} is the innermost stable orbit. Assuming the BH's spin is prograde with respect to the accretion disc,

R_{ISCO} is given by

$$R_{\text{ISCO}} = 3 + r_2 - \sqrt{(3 - r_1) \times (3 + r_1 + 2 \times r_2)}, \quad (13)$$

in units of GM/c^2 and r_1 and r_2 are given by

$$r_1 = 1 + (1 - a^2)^{1/3}(1 + a)^{1/3} + (1 - a)^{1/3}, \quad (14)$$

$$r_2 = \sqrt{3a^2 + r_1^2}, \quad (15)$$

and a is the dimensionless black hole spin, assumed to be 0.7. These assumptions lead to a radiative efficiency $\epsilon \sim 0.1$.

When the accretion rate exceeds the Eddington limit, we swap to a slim disc model as in [Madau et al. \(2014\)](#), where generated heat is efficiently radiated away and ϵ is appropriately reduced from the sub-Eddington value, weakening BH feedback. We calculate the Eddington accretion limit as

$$\dot{M}_{\text{Edd}} = \frac{4\pi GMm_p}{\epsilon c\sigma_T}, \quad (16)$$

where G is the gravitational constant, c is the speed of light, ϵ is the sub-Eddington value calculated using Equation 12 and $\sigma_T = 6.65 \times 10^{-25} \text{ cm}^2$ is the Thomson scattering cross-section for an electron.

In the super-Eddington regime, we first calculate the Eddington luminosity as

$$L_{\text{Edd}} = \frac{4\pi GMm_p\mu c}{\sigma_T}, \quad (17)$$

where μ is the mean molecular weight, assumed to be 1.22. We then use the parametrization found in [Madau et al. \(2014\)](#) to calculate the super-Eddington luminosity

$$L_{\text{SE}} = L_{\text{Edd}} A \left(\frac{0.985}{r_{\text{Edd}} + B} + \frac{0.015}{r_{\text{Edd}} + C} \right), \quad (18)$$

where r_{Edd} is the ratio of the accretion rate to the Eddington limit, and

$$\begin{aligned} A &= (0.9663 - 0.9292a)^{-0.5639}, \\ B &= (4.627 - 4.445a)^{-0.5524}, \\ C &= (827.3 - 718.1a)^{-0.7060}, \end{aligned} \quad (19)$$

where again the BH spin a is set to 0.7. The value of ϵ in the super-Eddington case then follows as

$$\epsilon = L_{\text{SE}} / (\dot{M}c^2). \quad (20)$$

Implementing this parameterisation reduces the value of ϵ for super-Eddington cases, thereby modulating the effective feedback injection at high accretion rates. We calculate the super-Eddington feedback energy by using the updated value of ϵ in Equation 11. For numerical stability, we limit the amount of energy that can be injected into a gas cell in any one timestep to be five times the current internal energy of the cell.

2.3. Dynamical Friction

Dynamical friction is the drag force experienced by heavy particles moving through a background sea of lighter dark matter particles, stars, and gas, causing the orbits to decay towards the gravitational potential minima ([Chandrasekhar 1943](#); [Binney & Tremaine 2011](#)).

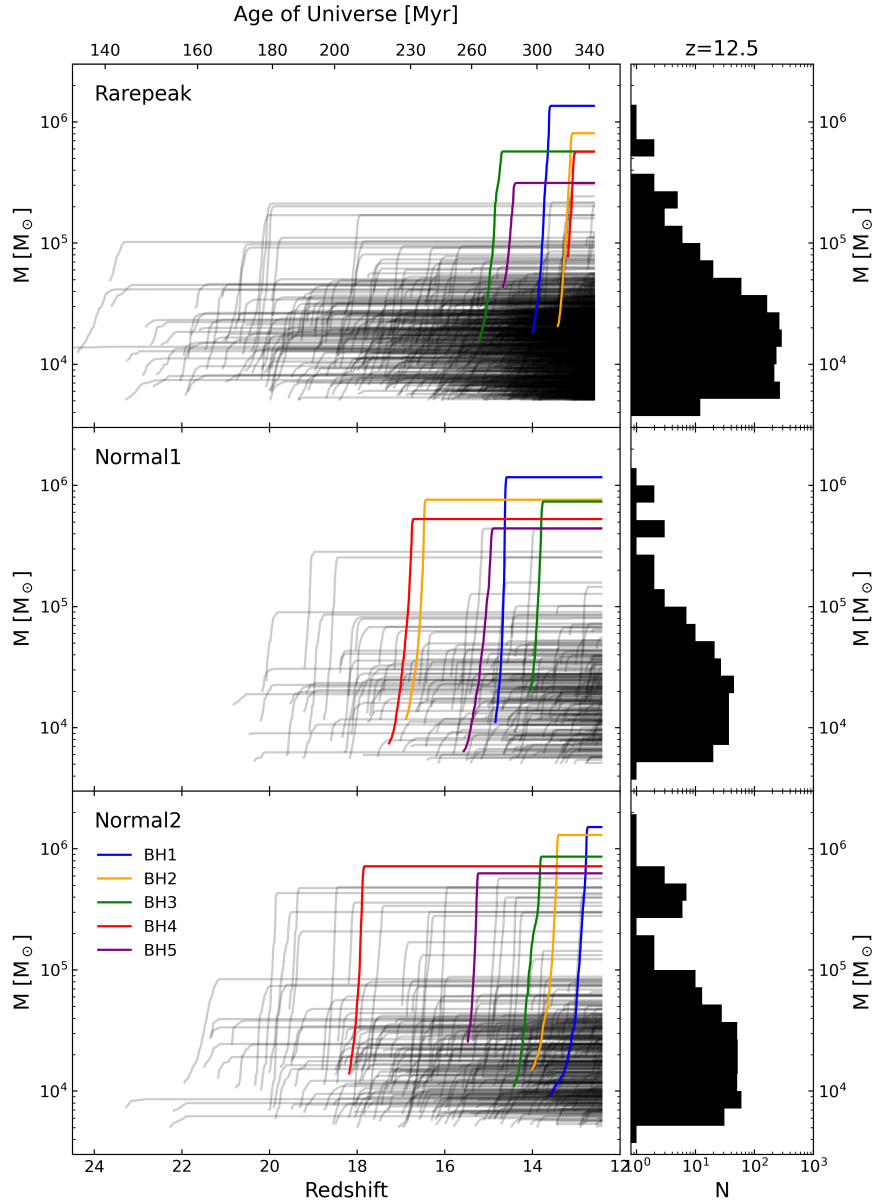


FIG. 1.— The growth of the most massive black holes across each of the three SEEDZ volumes (RAREPEAK, NORMAL1, NORMAL2). Each simulation has now reached $z = 12.5$, with the most massive MBH in each realization now above $10^6 M_\odot$. The majority of MBHs however lie within a factor of a few of their initial seed mass. We show the growth history of the top 5 most massive MBHs in each realisation as colored lines.

In cosmological simulations, large dark matter particle masses make it hard to resolve gravitational friction and also leads to unphysical gravitational heating, due to two-body encounters between particles. In order to avoid this numerical heating, gravitational interactions between particles are damped below a specified gravitational softening length (Governato et al. 1994; Kazantzidis et al. 2005). However, this has the side effect of reducing the dynamical friction acting on the heavy particles. To correct for this effect, we include an additional acceleration term acting on the BH particles, that accounts for gravitational interactions that are artificially suppressed by the softening. The volume over which interactions are suppressed is $V_s = 4/3\pi r_s^3$, where $r_s = 3.1$

ckpc/h is the softening length for BH particles. This softening remains constant and does not change with time or local properties around the BH particles. The softening length for BH particles is ~ 20 times larger than the minimum resolution of gas cells.

We build our dynamical friction model based on Tremmel et al. (2015), adding it to AREPO2. We assume that the velocity dispersion of particles within the radius r_s is isotropic and that the classical Chandrasekhar treatment of dynamical friction applies (Chandrasekhar 1943). We further assume that only particles moving slower than the BH would influence its motion, giving us an acceleration of the form

$$a_{\text{DF}} = -4\pi G^2 M_{\text{BH}} \rho (< v_{\text{BH}}) \ln \Lambda \frac{v_{\text{BH}}}{|v_{\text{BH}}^3|} \quad (21)$$

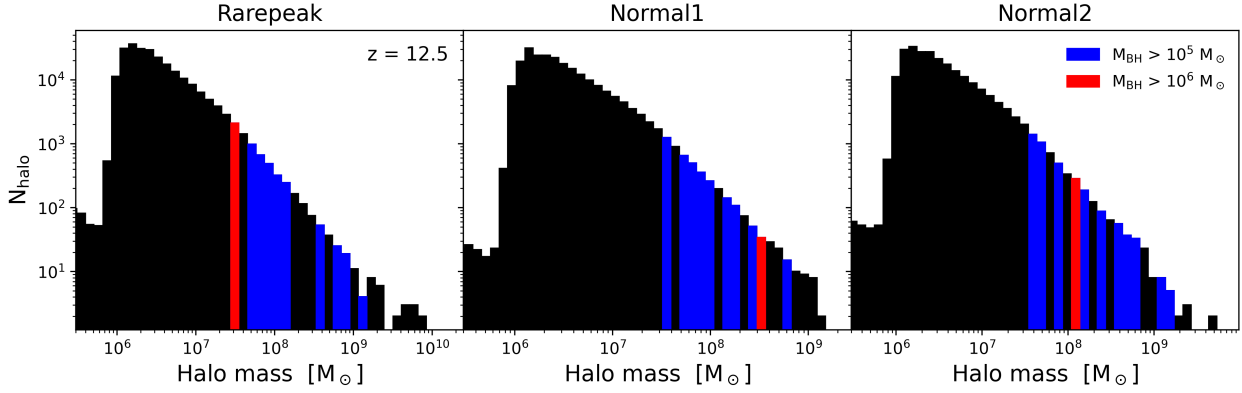


FIG. 2.— Halo mass functions (HMFs) for the 3 simulation regions at $z = 12.5$. We colour mass bins containing MBHs of mass greater than 10^5 and $10^6 M_\odot$ in blue and red, respectively. Note that the heights of these coloured bins have not been altered from the original HMF, therefore the heights do not indicate number of halos containing MBHs.

where $\rho(< v_{\text{BH}})$ is the density of background particles moving slower than than the BH and v_{BH} is the velocity of the BH. The Coulomb logarithm, $\ln \Lambda$, depends on the maximum and minimum impact parameters, b_{max} and b_{min} , as $\Lambda = b_{\text{max}}/b_{\text{min}}$. Since gravitational interactions beyond the softening length are well resolved, we take $b_{\text{max}} = r_s$ in order to avoid any over-counting of the effects of dynamical friction. For the minimum impact parameter, we take the radius of the influence for the BH, i.e.

$$b_{\text{min}} = \frac{GM_{\text{BH}}}{v_{\text{BH}}^2}. \quad (22)$$

For the purpose of this study, only dynamical friction from dark matter particles is taken into consideration when computing this correction. The dynamical friction from stars will be small at our current resolution and was neglected for this work, but will be added in future versions of the model. In addition, we only employ dynamical friction for BHs whose mass is larger than 5 times the dark matter particle mass ($\sim 3.45 \times 10^5 h^{-1} M_\odot$), as the dynamics can be hindered further by applying the correction when $M_{\text{BH}} \sim M_{\text{DM}}$. For BHs with masses comparable to individual dark matter particles, the resulting dynamical friction becomes noisy and dominated by stochastic fluctuations (Tremmel et al. 2015). The resulting acceleration is added to the BH acceleration to be integrated over the next time-step. As the mass of the BH increases, the radius of influence grows and can eventually become larger than b_{max} . Once this happens, we assume that dynamical friction is fully resolved and no longer include this correction term.

2.4. Stellar and Black Hole Mergers

We allow black hole particles to merge based on the treatment originally implemented in Prole et al. (2022). SmartStar particles are merged if:

- They lie within each other's accretion radius of 0.62 ckpc h^{-1} .
- They are moving towards each other.
- Their relative accelerations are < 0 .
- They are gravitationally bound to each other.

As our BH particles carry no thermal data, the last criterion simply requires that their gravitational potential exceeds the kinetic energy of the system. When these criteria are met, the larger of the particles gains the mass and linear momentum of the smaller particle, and its position is shifted to the centre of mass of the system. Comparing the accretion radius of 0.62 ckpc h^{-1} to the sink particle gravitational softening length of 3.1 ckpc h^{-1} means that mergers will likely be somewhat suppressed within this initial suite of 'low resolution' calibration runs.

3. RESULTS

In Figure 1 we show the growth evolution of all heavy seed MBHs in the RAREPEAK, NORMAL1 and NORMAL2 simulation suites, down to $z = 12.5$. In each case, the most massive black hole reached a mass of just over $10^6 M_\odot$, with most MBHs lying within a factor of a few of their initial seed mass. A significant fraction of the MBHs experienced periods of rapid growth before a sudden accretion cut-off, which is particularly true for the most massive MBHs in each case. We show the halo mass functions (HMFs) in Figure 2, which indicate that our most massive MBHs do not reside in the most massive halos (10^9 - $10^{10} M_\odot$), but rather within halos with masses ranging from a few times $10^7 M_\odot$ to a few times $10^8 M_\odot$. Here, we investigate the growth of these MBHs, and defer the examination of the host halo's formation history and their positioning with respect to the greater cosmic web to a follow-up paper. In the following subsections, we investigate the physical mechanism that prevents these MBHs from growing beyond approximately $10^6 M_\odot$, by inspecting their environments and host halo properties, before, during and after the accretion cut off.

3.1. What sets the final mass of the most massive black holes?

From a purely numerical perspective, accretion will end when there is a lack of cold, dense gas within the accretion radius of a MBH. There are a number of physical reasons why this may occur: A) MBHs may simply accrete all of the available gas; B) MBH accretion feedback could heat the surrounding gas and severely suppress accretion; C) nearby SNe explosions can evacuate the gas from around a MBH; D) gravitational interactions could eject a MBH from its accretion supply, or E) the dense

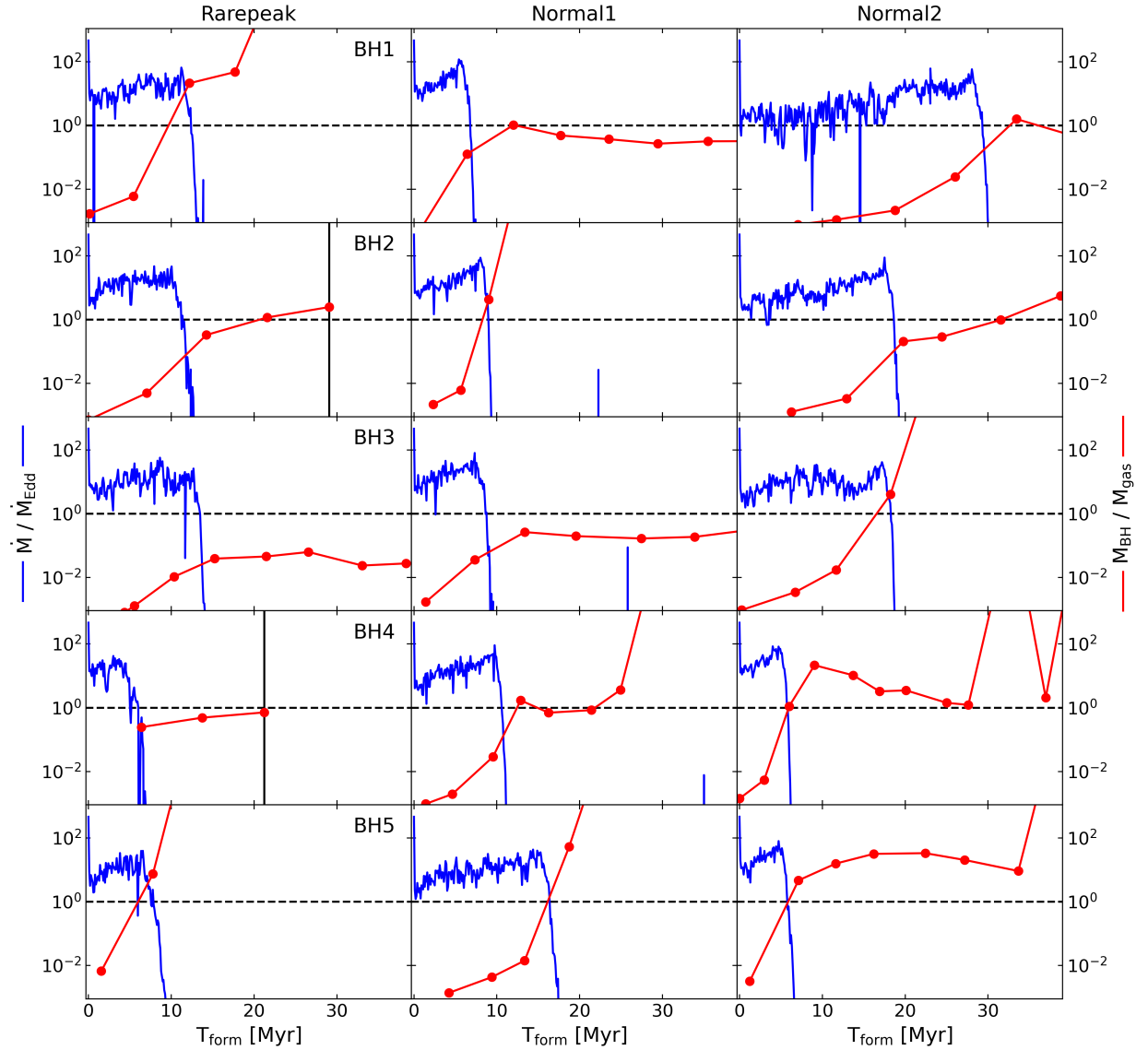


FIG. 3.— For the top 5 most massive MBHs by $z = 12.5$ in each simulation, we show the MBH growth rate expressed as the ratio of the accretion rate to the Eddington rate, as a function of time since the formation of the MBH (blue). We also show the ratio of the mass of the MBH to the remaining gas mass within its host halo (red), as identified with the Subfind halo finder. We show the end point of the simulations as a black vertical line where appropriate.

gas may instead form stars and other MBHs rather than be accreted onto the MBH. In this section, we will disentangle these mechanisms to find out which one (or what combination) drives this process in SEEDZ.

Figure 3 shows the MBH growth rate for the top 5 most massive MBHs in each simulation, displayed as the ratio of the accretion rate to the Eddington accretion rate. In each case, super-Eddington accretion lasts for up to a few tens of Myr before experiencing a sharp decrease in growth. In each case, we identify the MBH’s host halo using AREPO’s built-in halo finder, Subfind (Springel et al. 2021). The Figure also shows the gas mass within the virial radius of each of these host halos, which also drops substantially prior to the accretion cut-off in all cases. At the time when the MBHs transitioned from super- to sub-Eddington accretors, the remaining gas mass within each halo has become comparable/much lower than that

of the accreting MBH. This raises the question of whether the removed gas mass had been accreted onto the MBH, if the gas had formed into new stars/BHs within the halo, or if the gas was evacuated from each halo by a feedback process.

To investigate this, Figure 4 shows the total mass in all stars and BHs within each of these halos, along with its total remaining gas mass, at the time when accretion was cut off. As the gas mass within each halo decreased, the mass in BHs and stars did not increase to match the deficit, falling short by an order of magnitude. This clearly shows that gas was evacuated from each halo, rather than being accreted or forming new objects.

3.2. Black hole feedback versus supernovae feedback

Given that most of the halo’s gas was evacuated from the halo at approximately the same time as its cen-

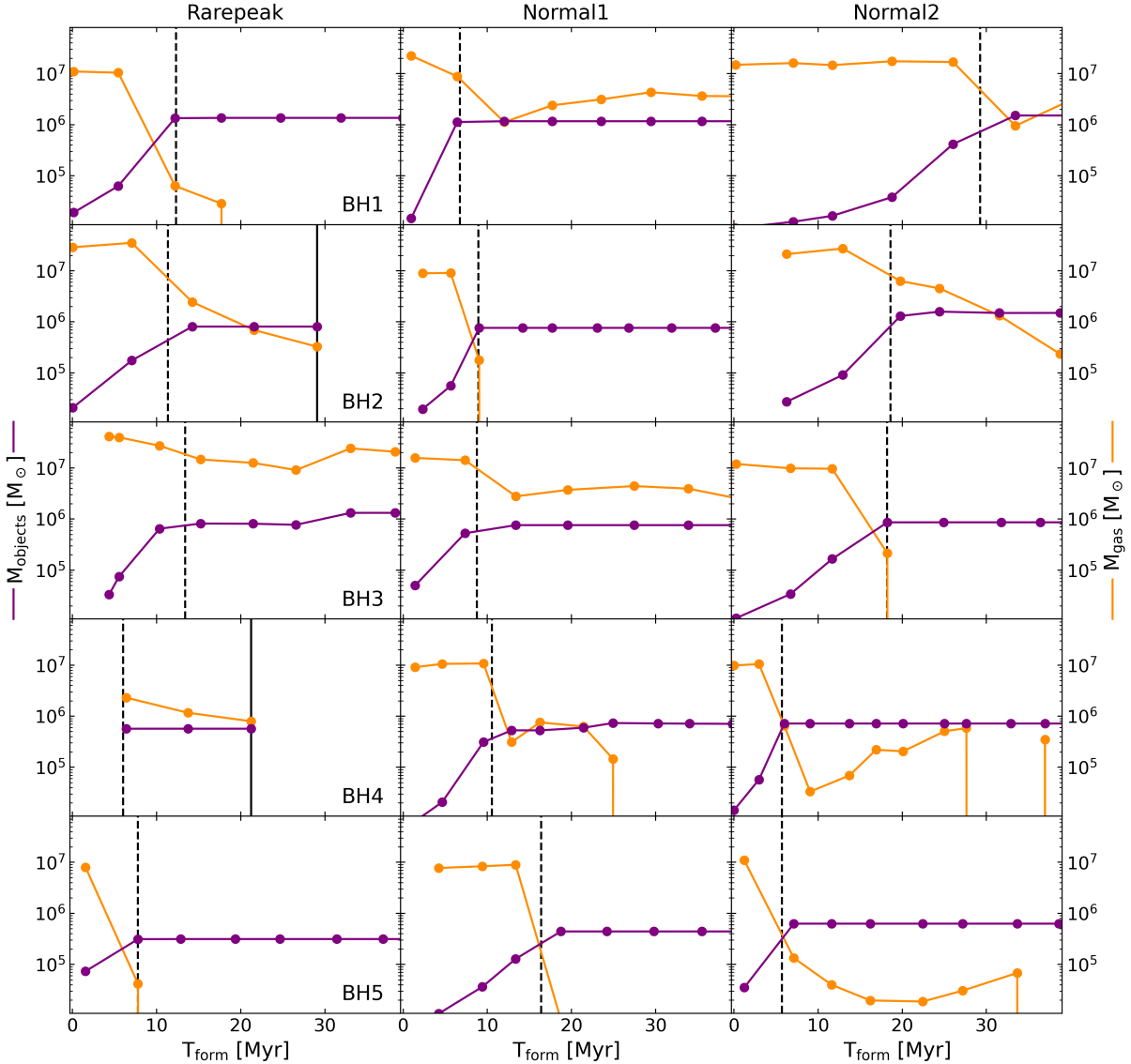


FIG. 4.— For the top 5 most massive MBHs by $z = 12.5$ in each simulation, we show the combined mass in all stars and BHs within its host halo, as a function of time since the formation of the central MBH (purple). We also show the remaining gas mass within the halo (orange). Note that this data was taken from snapshots, with a lower output frequency than the black hole data shown in Figure 3. We show the point where the MBH transitions from super- to sub-Eddington growth as a vertical dashed line, and show the end point of the simulations as a black vertical line where appropriate. As MBH accretion shuts off, the combined mass in stars and MBHs does not increase. Therefore, the formation of additional stars and/or MBHs is not responsible for cutting off the primary MBH’s accretion supply.

tral MBH stopped accreting, two mechanisms may have driven this process. Either the thermal accretion feedback injected into the MBH’s immediate surroundings heated the gas to such an extent that it expanded out to radii larger than the halo’s virial radius (at very low gas densities), or SN explosions from nearby stars pushed the gas out of the halo via our momentum based SNe prescription.

To differentiate between these two possibilities, we have identified halos with no stellar formation or SNe activity between the time of MBH formation and the subsequent accretion cut-off. In Figure 5 we plot density and temperature projections around N1BH1 (NORMAL1 black hole 1), see appendix A.10 and A.11 for more examples from N2BH3 and N2BH4. The panels from left

to right show snapshots immediately before, during and after the accretion is cut off. In the absence of SNe explosions, the gas component of the halo was significantly disrupted purely by BH accretion feedback, which heated the gas up to 10^6 - 10^7 K on scales larger than the virial radius of the halo. The region of hot gas grew as the dense gas became more diffuse, spreading out to scales of ~ 20 kpc before dropping in temperature to 10^5 K. The bottom row also encompasses a neighboring halo, which did experience SNe explosions but lacked a growing MBH. This neighboring halo only reached maximum temperatures of up to $\sim 10^5$ K due to SNe feedback alone.

To emphasize that this outflow behavior is caused by MBH feedback rather than from SNe explosions, we also examine halos in our simulations that house large stellar

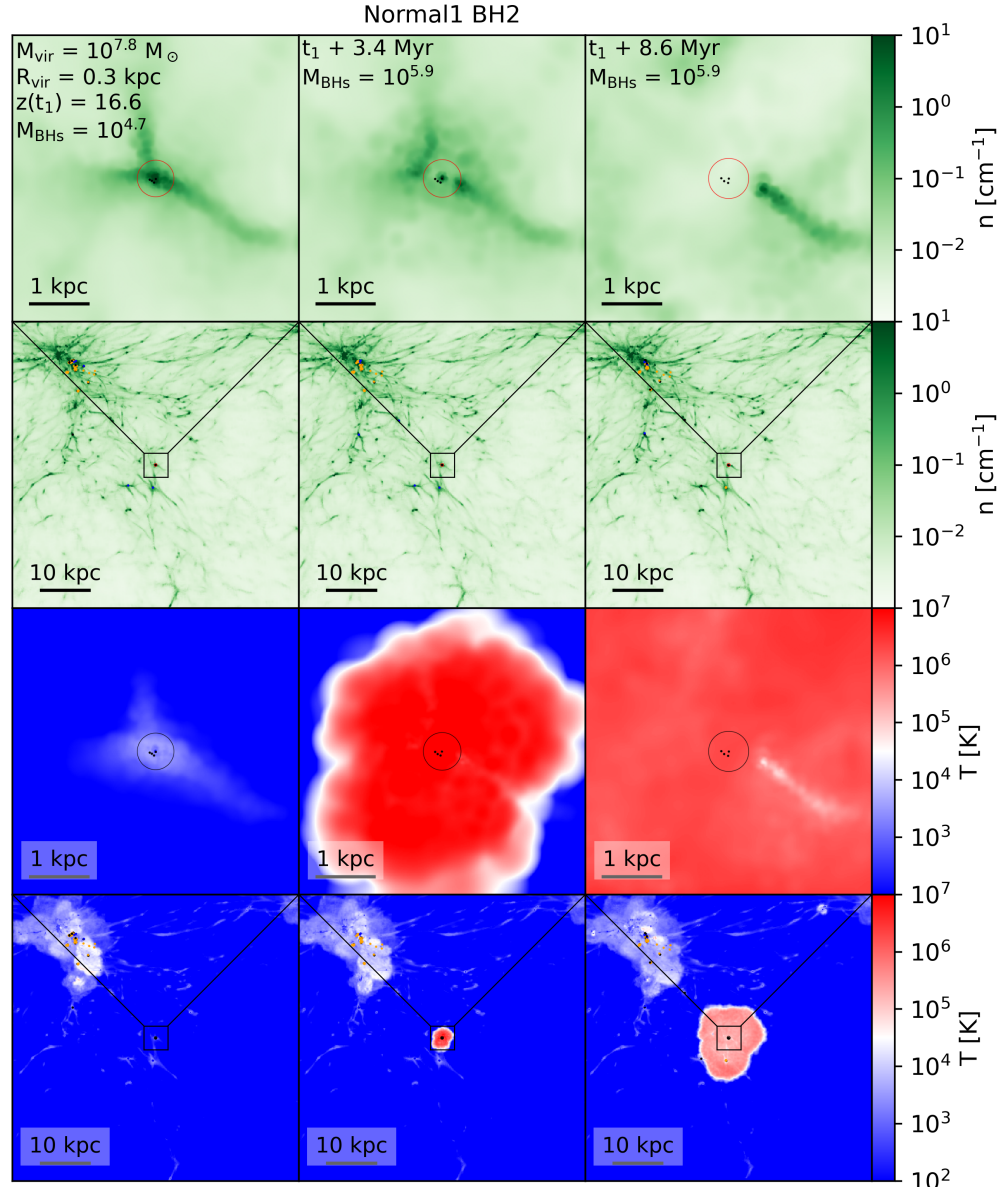


FIG. 5.— Projections of the halo containing N1BH2 before (left), during (center) and after (right) the accretion cut-off. The top 2 panels show density projections, while the bottom 2 panels show temperature projections. Scale lines are given in each panel to indicate the scale of each projection. BHs, PopIII stars and PopII stellar cluster particles are shown as black, blue and orange dots, respectively. We show the virial radius of the halo as a circle. We include values for the virial mass, virial radius, redshift and black hole mass.

populations. Figure 6 shows projections from the halo with the largest gas mass in each simulation. These halos house BHs which are sub-dominant compared to the stellar mass. In particular, we examine a halo in the RAREPEAK simulation which has a virial mass of $10^{10.1} M_{\odot}$, a host gas mass of $10^{9.2} M_{\odot}$, a stellar mass of $10^{7.4} M_{\odot}$ and a total BH mass of $10^{5.6} M_{\odot}$. In the NORMAL1 simulation, the halo has a virial mass of $10^{9.1} M_{\odot}$, a host gas mass of $10^{8.2} M_{\odot}$, a stellar mass of $10^{6.5}$ and a total BH mass of $10^{4.1} M_{\odot}$. Finally, the NORMAL2 halo has a virial mass of $10^{9.7} M_{\odot}$, a host gas mass of $10^{8.8} M_{\odot}$, a stellar mass of $10^{6.9} M_{\odot}$ and a total BH mass of $10^{5.1} M_{\odot}$. In these halos where the stellar mass is dominant and the BHs are not actively accreting, the galaxies are

not quenched and the gas component has not been thermally expanded by SNe feedback compared to the AGN feedback seen in Figure 5.

3.3. Galaxy disruption and determining the maximum black hole masses

It is now clear that MBH accretion feedback causes the sharp accretion cut-off experienced by the MBHs in the SEEDZ simulations. We now post-process the simulation outputs to explain why the MBHs grow so rapidly and why the feedback is so destructive. In Figure 7, we highlight N2BH1, as it has the most snapshot outputs between the formation of the MBH and its accretion cut-off (see Appendix Figure A.12 for further ex-

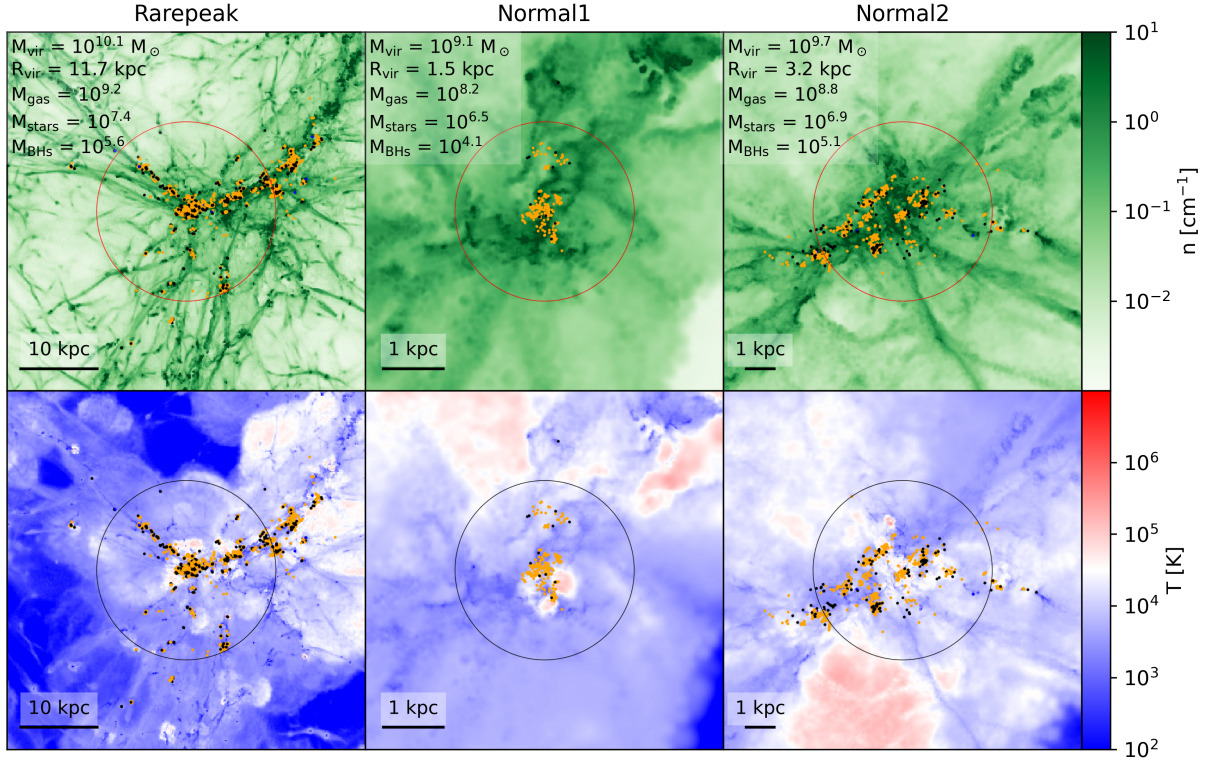


FIG. 6.— Density (top) and temperature (bottom) projections of the halo with the highest gas mass at $z = 12.5$ in each simulation. We match the colorbar to the previous figure to demonstrate the significantly lower temperatures in these halos. BHs, PopIII stars and PopII clusters are shown as black, blue and orange dots, respectively. The halo virial radius is shown as a circle. We also include values for the halo virial mass, virial radius, gas mass, stellar mass and total black hole mass.

amples). The top 3 panels show quantities relevant for calculating the accretion rate using equation 2, showing the mass weighted average densities, velocities and temperatures within the accretion sphere surrounding the MBH. Using these values and equation 2, we estimate the accretion rate in the 4th panel (red) and compare it to the accretion rate calculated on-the-fly within the simulation (blue), as described in §2.1. The combination of high densities, low velocities and temperatures allow for super-Eddington accretion rates, reaching over 10 times the Eddington rate at their peak.

The feedback radiative efficiency ϵ varies during super-Eddington accretion, given by equation 12, which is shown in panel 5 of Figure 3. The reduction of ϵ from its fixed sub-Eddington value allows for weaker feedback during periods of rapid (super-Eddington) growth. This further enables sustained super-Eddington accretion. We use these values of ϵ with equation 11 to estimate the energy injected into the gas surrounding the MBH during the $\sim 10^5$ yr data output intervals, which is plotted in the bottom panel of Figure 7. Note that the estimated energy is likely much larger than the real injected energy due to the injection cut-off described in §2.2. As the accretion rate continues to increase, the estimated energy injected during a single 10^5 yr time interval surpasses the entire binding energy of the halo, which we include as a dashed line for comparison.

The rapid accretion necessary to grow our seed black holes up to $10^6 M_\odot$ by $z = 12.5$, combined with the

binding energy of halos, given by

$$E_{\text{bind}} = \frac{3GM_{\text{vir}}^2}{5R_{\text{vir}}}, \quad (23)$$

effectively sets $10^6 M_\odot$ as the maximum mass a MBH can attain before super-Eddington feedback is sufficient to unbind the gas from its halo (which have masses of at most $10^{10} M_\odot$ at this epoch). This halo mass upper limit is therefore the defining factor in determining the final black hole masses in the SEEDZ simulations. Once the feedback energy released from rapidly accreting MBHs can not be contained by the gravitational energy of their host halos, the gas is fully evacuated and accretion stops. We therefore predict that galaxies at the epoch of $z \sim 10$ may show signs of significant quenching, unless the accretion feedback can be efficiently damped near to the MBH.

3.4. Halo outflows and long-term recovery

For a broader investigation into the outflow behavior discussed in §3.2, we plot inflow/outflow properties around each of the 5 most massive MBH's host halos in Figure 8. We take averaged quantities within a shell spanning from the halo virial radius R_{virial} , out to $1.5R_{\text{virial}}$, at the time of the accretion cutoff, T_{cutoff} . We show the mass inflow/outflow rate in the top panel of Figure 8 - in all cases, initial inflow rates were between $0.1 - 1 M_\odot \text{ yr}^{-1}$. At the time of the accretion cut-off, this positive inflow switched to a negative

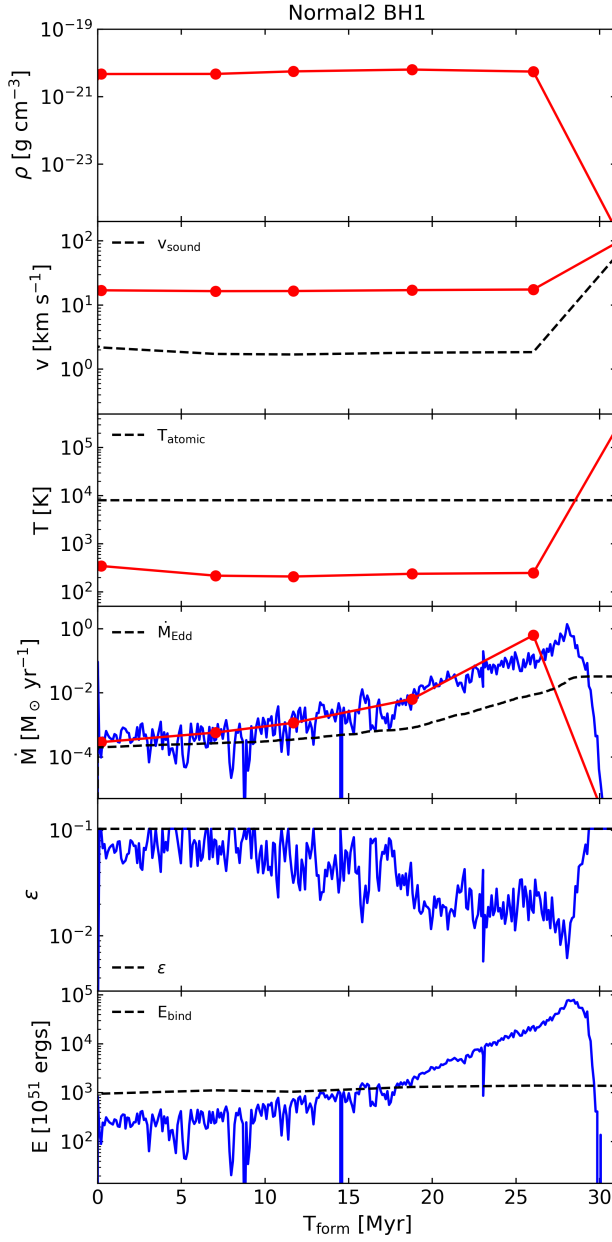


FIG. 7.— Accretion and feedback properties of the BH. The top 3 panels show mass weighted average density, relative velocity and temperature of the gas within the accretion sphere surrounding N2BH1. The sound speed is shown as a dashed line. The 4th panel shows the accretion rate onto the BH (blue) and the rate estimated from the properties in the top 3 panels (red). The 5th panel shows the feedback parameter ϵ during the super-Eddington burst (blue), compared to the sub-Eddington value (dashed black). The bottom panel shows the energy injected in each timebin of roughly 10^5 (blue) compared to the binding energy of the halo (dashed black).

outflow, with highs of $10^{-1} M_\odot \text{ yr}^{-1}$, before slowing down towards a near stationary flow ($0 M_\odot \text{ yr}^{-1}$)¹ on timescales of 5-10 Myr. This indicates that feedback from all of the considered MBHs thermally expanded the gas component outside of their host halo's virial radii. To make predictions for possible observations

¹ Intriguingly recent LRD measurements show net inflow/outflow rates of zero (Sneppen et al. 2026) - we will return to this discussion point in §4

of such outflows surrounding growing MBHs, we plot the outflow velocities and temperatures in the middle and bottom panels. At the point where accretion ends, gas outflows at 10^3 km s^{-1} , generally slowing to 10 km s^{-1} on timescales of 10 Myr. These outflows reach temperatures of 10^7 K at their peak, cooling to 10^5 K in the following 10-20 Myr.

Despite exhibiting prominent outflows, many of these halos do eventually recover and reach inflow rates comparable to the pre-outflow values. Figure 9 shows the mass inflow rates over a longer timeframe, running from the MBH's creation to the end of the simulation at $z = 12.5$. Some of these systems recover inflow rates of $0.1 M_\odot \text{ yr}^{-1}$ on short timescales of 20-40 Myr (RAREPEAK BH1,3,5 and NORMAL1 BH1,3,4), while others recover after roughly 100 Myr (NORMAL1 BH4, NORMAL2 BH4). However, for many of these MBHs, there is not enough time between the outflow period and the end of the simulation to begin inflowing. For example NORMAL1 BH2 and BH5 remain at net zero mass inflow for almost 100 Myr. Even in systems that do regain their high inflow rates, the MBH does not experience another growth phase by the end of the simulation. However, MBH accretion is likely to re-occur if given more time. As our simulations continue to evolve, we will return to this point in a follow-up work.

4. DISCUSSION & CONCLUSIONS

In this paper, we have analysed the growth and feedback properties of the most massive BHs in the SEEDZ simulations, yielding a number of important conclusions, listed below:

- In a cosmological setting, heavy seed BHs with initial masses between 5×10^3 and $10^5 M_\odot$ are capable of growing into $10^6 M_\odot$ SMBHs by $z = 12.5$
- The most massive MBHs gain their mass during short periods of super-Eddington accretion lasting between 5-30 Myr.
- The most active and massive MBHs in our suite inject significant thermal energy into their surroundings to unbind the gas from its host halo. The rapid accretion and resulting strong feedback effectively quenches the host galaxy. This sets a maximum MBH mass at this epoch (determined by the binding energy and hence mass of the host halo). Our simulations predict maximum MBH masses of approximately $10^6 M_\odot$ at $z = 12.5$.
- Either MBH feedback in the early Universe is much less efficient than our model, or the MBHs we observe with JWST may have evacuated their host halo's gas reservoir during their formation, and later built up a stellar component following replenishment of their gas reservoir from the cosmic web or through halo mergers.

The goal of this paper was to examine the growth and limitations of MBHs in the SEEDZ simulation suite. Our main finding is that MBHs are unlikely to exceed approximately $10^6 M_\odot$ through accretion alone by $z = 12.5$.

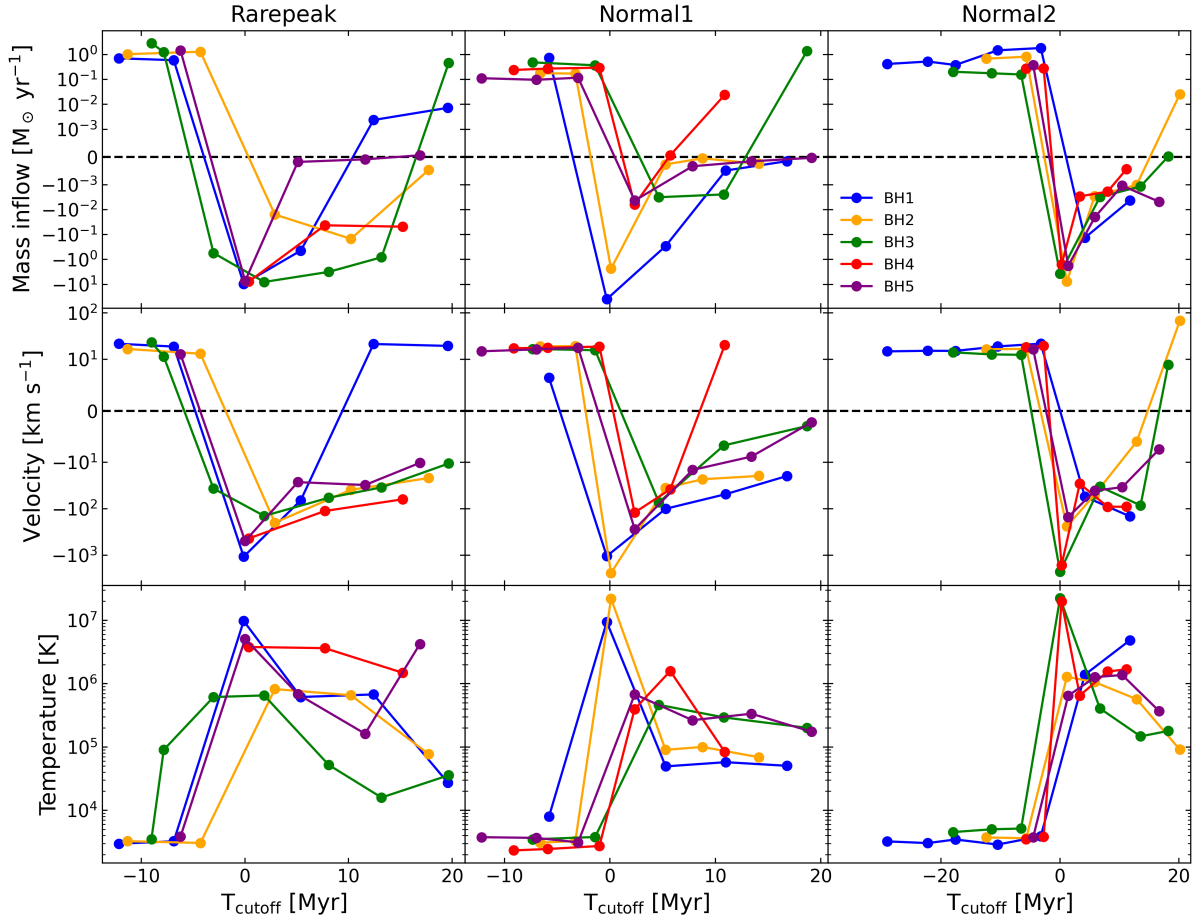


FIG. 8.— The time evolution of halo outflow properties at the time of the MBH accretion cut-off, sampled within a shell extending from the virial radius R_{vir} out to $1.5R_{\text{vir}}$. Top - Gas mass inflow (positive) and outflow (negative) rates, given by the sum of contributions from all cells within the shell. Middle - mass weighted average radial velocities, relative to the central MBH. Bottom - mass weighted average temperatures within the shell. The x -axis shows the time before and after the accretion cut-off, T_{cutoff} .

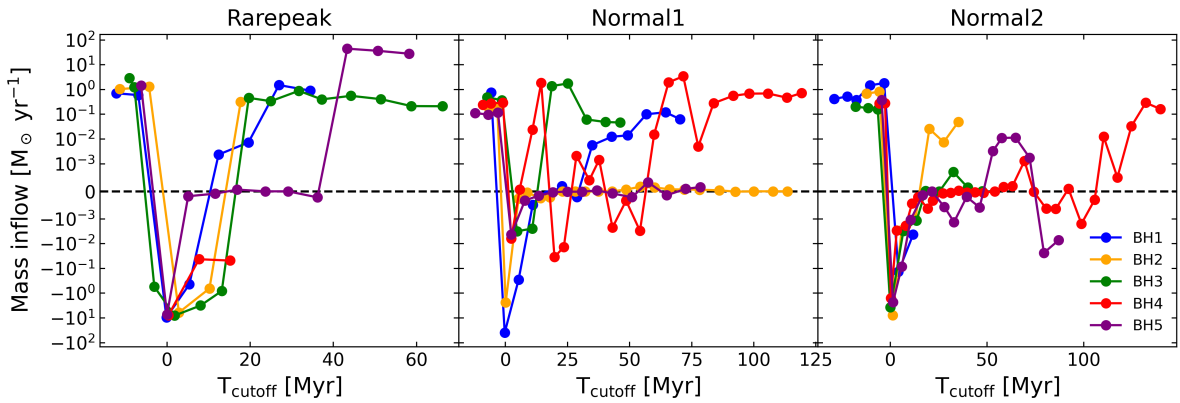


FIG. 9.— The top panel of Figure 8, but with the x -axis extended in time to encompass the time remaining until the end of the simulation. We show gas mass inflow (positive) and outflow (negative) rates, given by the sum of contributions from all cells within a shell extending from R_{vir} out to $1.5R_{\text{vir}}$. The plot shows that many of the MBH's host halos recover from their outflow phase and begin to experience inflow rates comparable to the pre-outflow rates, although none of the MBHs experience a second accretion phase by the end of the simulation.

The associated feedback injected into the inter-stellar medium due to rapid accretion unbinds the gas from the host halo. In principle, this tells us that any future observations of MBHs with masses significantly larger than $10^6 M_\odot$ before $z = 12.5$ would have major implications for our models of the early Universe. Of course, this assumes that our model for MBH accretion and feedback captures the key physical processes and is numerically converged.

The feedback model implemented in the SEEDZ simulations injects thermal feedback isotropically into the surrounding medium during accretion episodes. It is entirely possible that our feedback model and parameters are too strong. However, the feedback prescription is already relatively weak, employing thermal feedback with a gas coupling factor of 0.05, and further reducing the radiative efficiency ϵ during super-Eddington phases, as described in §2.2. In a forthcoming study, we will explore the parameter space of these feedback parameters.

4.1. Observational Guidance from Little Red Dots

Recent observations of so-called Little-Red-Dot (LRD) (Matthee et al. 2024) systems offer potential observational guidance to our theoretical models. If LRDs are systems with dense gas surrounding a rapidly accreting MBH at the center (e.g. Inayoshi & Maiolino 2025; Inayoshi et al. 2025; Naidu et al. 2025; de Graaff et al. 2025a,b; Rusakov et al. 2025, 2026; Sun et al. 2026) as they appear to be, then our feedback modeling may require some adjustment. The observed systems hosting LRDs have total (virial) masses not significantly beyond our largest halo masses, in the region of approximately $10^{11} M_\odot$ (our most massive halos will reach masses in excess of this by $z = 10$). Our modeling suggests that such halos should show significant signs of galaxy quenching. Observations thus far do not support this (e.g. Sneppen et al. 2026), suggesting that dense gas surrounding growing MBHs is able to contain the feedback energy. The increased resolution in our upcoming suite of follow-up simulations may result in LRD-like systems, as the increased resolution will allow for higher densities surrounding growing MBHs and therefore a possibly different feedback result. Nonetheless, early observations from LRDs (assuming they host small but actively accreting MBHs) suggest that feedback in these early galaxies does not disrupt the host halo, despite the necessarily high accretion rates. Hence, higher resolution models coupled with further observational guidance will be required to understand MBHs in the early Universe.

ACKNOWLEDGEMENTS

JR & JB acknowledges support from the Royal Society and Research Ireland under grant number URF\R1\191132. LP, DM & JR acknowledge support from the Research Ireland Laureate programme under grant number IRCLA/2022/1165. JHW acknowledges support from NSF grants AST-2108020 and AST-2510197 and NASA grant 80NSSC21K1053. RSB acknowledges support from a UKRI Future Leaders Fellowship MR/Y015517/1. The simulations were performed on the Luxembourg national supercomputer MeluXina

and the Czech Republic EuroHPC machine Karolina. The authors gratefully acknowledge the LuxProvide teams for their expert support. The authors wish to acknowledge the Irish Centre for High-End Computing (ICHEC) for the provision of computational facilities and support. The authors acknowledge the EuroHPC Joint Undertaking for awarding this project access to the EuroHPC supercomputer Karolina, hosted by IT4Innovations through a EuroHPC Regular Access call (EHPC-REG-2023R03-103) and to the LuxProvide supercomputer Meluxina through a EuroHPC Regular Access call (EHPC-REG-2025R01-008). S.K. acknowledges support from the Royal Society under grant number URF\R1\251867 and the Royal Commission for the Exhibition of 1851. M.A.B. is supported by a UKRI Stephen Hawking Fellowship (EP/X04257X/1). RSK acknowledges financial support from the ERC via Synergy Grant “ECOGAL” (project ID 855130) and from the German Excellence Strategy via the Heidelberg Cluster “STRUCTURES” (EXC 2181 - 390900948). In addition RSK is grateful for funding from the German Ministry for Economic Affairs and Climate Action in project “MAINN” (funding ID 50OO2206), and from DFG and ANR for project “STARCLUSTERS” (funding ID KL 1358/22-1).

REFERENCES

Agarwal, B., Dalla Vecchia, C., Johnson, J. L., Khochfar, S., & Paardekooper, J.-P. 2014, Monthly Notices of the Royal Astronomical Society, 443, 648, doi: [10.1093/mnras/stu1112](https://doi.org/10.1093/mnras/stu1112)

Agarwal, B., Khochfar, S., Johnson, J. L., et al. 2012, Monthly Notices of the Royal Astronomical Society, 425, 2854, doi: [10.1111/j.1365-2966.2012.21651.x](https://doi.org/10.1111/j.1365-2966.2012.21651.x)

Alvarez, M. A., Wise, J. H., & Abel, T. 2009, The Astrophysical Journal, 701, L133, doi: [10.1088/0004-637X/701/2/L133](https://doi.org/10.1088/0004-637X/701/2/L133)

Ardaneh, K., Luo, Y., Shlosman, I., et al. 2018, Monthly Notices of the Royal Astronomical Society, 479, 2277, doi: [10.1093/mnras/sty1657](https://doi.org/10.1093/mnras/sty1657)

Becerra, F., Greif, T. H., Springel, V., & Hernquist, L. E. 2015, Monthly Notices of the Royal Astronomical Society, 446, 2380, doi: [10.1093/mnras/stu2284](https://doi.org/10.1093/mnras/stu2284)

Begelman, M. C., & Rees, M. J. 1978, Monthly Notices of the Royal Astronomical Society, 185, 847, doi: [10.1093/mnras/185.4.847](https://doi.org/10.1093/mnras/185.4.847)

Begelman, M. C., Rossi, E. M., & Armitage, P. J. 2008, MNRAS, 387, 1649, doi: [10.1111/j.1365-2966.2008.13344.x](https://doi.org/10.1111/j.1365-2966.2008.13344.x)

Begelman, M. C., Volonteri, M., & Rees, M. J. 2006, MNRAS, 370, 289, doi: [10.1111/j.1365-2966.2006.10467.x](https://doi.org/10.1111/j.1365-2966.2006.10467.x)

Binney, J., & Tremaine, S. 2011, Galactic Dynamics (Princeton university press)

Bogdán, Á., Goulding, A. D., Natarajan, P., et al. 2024, Nature Astronomy, 8, 126, doi: [10.1038/s41550-023-02111-9](https://doi.org/10.1038/s41550-023-02111-9)

Bondi, H. 1952, Monthly Notices of the Royal Astronomical Society, 112, 195, doi: [10.1093/mnras/112.2.195](https://doi.org/10.1093/mnras/112.2.195)

Booth, C. M., & Schaye, J. 2009, Monthly Notices of the Royal Astronomical Society, 398, 53, doi: [10.1111/j.1365-2966.2009.15043.x](https://doi.org/10.1111/j.1365-2966.2009.15043.x)

Carniani, S., Hainline, K., D'Eugenio, F., et al. 2024, Nature, 633, 318, doi: [10.1038/s41586-024-07860-9](https://doi.org/10.1038/s41586-024-07860-9)

Cenci, E., & Habouzit, M. 2025, Monthly Notices of the Royal Astronomical Society, 542, 2597, doi: [10.1093/mnras/staf1362](https://doi.org/10.1093/mnras/staf1362)

Chandrasekhar, S. 1943, The Astrophysical Journal, 97, 255, doi: [10.1086/144517](https://doi.org/10.1086/144517)

Chiaki, G., Chon, S., Omukai, K., et al. 2023, Monthly Notices of the Royal Astronomical Society, 521, 2845, doi: [10.1093/mnras/stad689](https://doi.org/10.1093/mnras/stad689)

Dattathri, S., Natarajan, P., Porras-Valverde, A. J., et al. 2025, ApJ, 984, 122, doi: [10.3847/1538-4357/adbeef](https://doi.org/10.3847/1538-4357/adbeef)

Dayal, P. 2024, Astronomy and Astrophysics, 690, A182, doi: [10.1051/0004-6361/202451481](https://doi.org/10.1051/0004-6361/202451481)

de Graaff, A., Hviding, R. E., Naidu, R. P., et al. 2025a, arXiv e-prints, arXiv:2511.21820, doi: [10.48550/arXiv.2511.21820](https://doi.org/10.48550/arXiv.2511.21820)

de Graaff, A., Rix, H.-W., Naidu, R. P., et al. 2025b, *A&A*, 701, A168, doi: [10.1051/0004-6361/202554681](https://doi.org/10.1051/0004-6361/202554681)

Fragione, G., & Leigh, N. 2018, *Monthly Notices of the Royal Astronomical Society*, 480, 5160, doi: [10.1093/mnras/sty2233](https://doi.org/10.1093/mnras/sty2233)

Gordon, S. T., Smith, B. D., Khochfar, S., & Beckmann, R. S. 2025, *Monthly Notices of the Royal Astronomical Society*, 537, 674, doi: [10.1093/mnras/staf054](https://doi.org/10.1093/mnras/staf054)

Gordon, S. T., Smith, B. D., Khochfar, S., & Regan, J. A. 2024, *Monthly Notices of the Royal Astronomical Society*, 529, 604, doi: [10.1093/mnras/stae566](https://doi.org/10.1093/mnras/stae566)

Governato, F., Colpi, M., & Maraschi, L. 1994, *Monthly Notices of the Royal Astronomical Society*, 271, 317, doi: [10.1093/mnras/271.2.317](https://doi.org/10.1093/mnras/271.2.317)

Habouzit, M., Volonteri, M., Latif, M., Dubois, Y., & Peirani, S. 2016, *Monthly Notices of the Royal Astronomical Society*, 463, 529, doi: [10.1093/mnras/stw1924](https://doi.org/10.1093/mnras/stw1924)

Haemmerlé, L., Klessen, R. S., Mayer, L., & Zwick, L. 2021, *Astronomy & Astrophysics*, 652, L7, doi: [10.1051/0004-6361/202141376](https://doi.org/10.1051/0004-6361/202141376)

Haemmerlé, L., Woods, T. E., Klessen, R. S., Heger, A., & Whalen, D. J. 2018, *Monthly Notices of the Royal Astronomical Society*, 474, 2757, doi: [10.1093/mnras/stx2919](https://doi.org/10.1093/mnras/stx2919)

Inayoshi, K., & Maiolino, R. 2025, *ApJ*, 980, L27, doi: [10.3847/2041-8213/adaebd](https://doi.org/10.3847/2041-8213/adaebd)

Inayoshi, K., Murase, K., & Kashiyama, K. 2025, Spectral Uniformity of Little Red Dots: A Natural Outcome of Coevolving Seed Black Holes and Nascent Starbursts, arXiv, doi: [10.48550/arXiv.2509.19422](https://doi.org/10.48550/arXiv.2509.19422)

Inayoshi, K., Visbal, E., & Kashiyama, K. 2015, *Monthly Notices of the Royal Astronomical Society*, 453, 1692, doi: [10.1093/mnras/stv1654](https://doi.org/10.1093/mnras/stv1654)

Juodžbalis, I., Maiolino, R., Baker, W. M., et al. 2024, *Nature*, 636, 594, doi: [10.1038/s41586-024-08210-5](https://doi.org/10.1038/s41586-024-08210-5)

Kashlinsky, A. 2021, *Phys. Rev. Lett.*, 126, 011101, doi: [10.1103/PhysRevLett.126.011101](https://doi.org/10.1103/PhysRevLett.126.011101)

Kazantzidis, S., Mayer, L., Colpi, M., et al. 2005, *The Astrophysical Journal*, 623, L67, doi: [10.1086/430139](https://doi.org/10.1086/430139)

Kovács, O. E., Bogdán, Á., Natarajan, P., et al. 2024, *The Astrophysical Journal Letters*, 965, L21, doi: [10.3847/2041-8213/ad391f](https://doi.org/10.3847/2041-8213/ad391f)

Krumholz, M. R., McKee, C. F., & Klein, R. I. 2004, *The Astrophysical Journal*, 611, 399, doi: [10.1086/421935](https://doi.org/10.1086/421935)

—. 2006, *The Astrophysical Journal*, 638, 369, doi: [10.1086/498844](https://doi.org/10.1086/498844)

Larson, R. L., Finkelstein, S. L., Kocevski, D. D., et al. 2023, *The Astrophysical Journal Letters*, 953, L29, doi: [10.3847/2041-8213/ace619](https://doi.org/10.3847/2041-8213/ace619)

Latif, M. A., Khochfar, S., Schleicher, D., & Whalen, D. J. 2021, *Monthly Notices of the Royal Astronomical Society*, 508, 1756, doi: [10.1093/mnras/stab2708](https://doi.org/10.1093/mnras/stab2708)

Latif, M. A., Schleicher, D. R. G., Schmidt, W., & Niemeyer, J. C. 2013, *Monthly Notices of the Royal Astronomical Society*, 436, 2989, doi: [10.1093/mnras/stt1786](https://doi.org/10.1093/mnras/stt1786)

Li, J., Silverman, J. D., Shen, Y., et al. 2024, arXiv preprint arXiv:2403.00074

Liu, B., Zhang, S., & Bromm, V. 2022, *Monthly Notices of the Royal Astronomical Society*, 514, 2376, doi: [10.1093/mnras/stac1472](https://doi.org/10.1093/mnras/stac1472)

Lodato, G., & Rice, W. K. M. 2004, *Monthly Notices of the Royal Astronomical Society*, 351, 630, doi: [10.1111/j.1365-2966.2004.07811.x](https://doi.org/10.1111/j.1365-2966.2004.07811.x)

Loeb, A., & Rasio, F. A. 1994, *The Astrophysical Journal*, 432, 52, doi: [10.1086/174548](https://doi.org/10.1086/174548)

Luo, Y., Ardaneh, K., Shlosman, I., et al. 2018, *Monthly Notices of the Royal Astronomical Society*, 476, 3523, doi: [10.1093/mnras/sty362](https://doi.org/10.1093/mnras/sty362)

Lupi, A., Haardt, F., Dotti, M., et al. 2016, *Monthly Notices of the Royal Astronomical Society*, 456, 2993, doi: [10.1093/mnras/stv2877](https://doi.org/10.1093/mnras/stv2877)

Madau, P., Haardt, F., & Dotti, M. 2014, *The Astrophysical Journal Letters*, 784, L38, doi: [10.1088/2041-8205/784/2/L38](https://doi.org/10.1088/2041-8205/784/2/L38)

Madau, P., & Rees, M. J. 2001, *The Astrophysical Journal*, 551, L27, doi: [10.1086/319848](https://doi.org/10.1086/319848)

Maiolino, R., Scholtz, J., Witstok, J., et al. 2024, *Nature*, 627, 59, doi: [10.1038/s41586-024-07052-5](https://doi.org/10.1038/s41586-024-07052-5)

Maiolino, R., Uebler, H., D'Eugenio, F., et al. 2025, A Black Hole in a Near-Pristine Galaxy 700 Million Years after the Big Bang, arXiv, doi: [10.48550/arXiv.2505.22567](https://doi.org/10.48550/arXiv.2505.22567)

Matthee, J., Naidu, R. P., Brammer, G., et al. 2024, *The Astrophysical Journal*, 963, 129, doi: [10.3847/1538-4357/ad2345](https://doi.org/10.3847/1538-4357/ad2345)

Matthee, J., Naidu, R. P., Kotiwale, G., et al. 2025, *The Astrophysical Journal*, 988, 246, doi: [10.3847/1538-4357/ade886](https://doi.org/10.3847/1538-4357/ade886)

Mayer, L., Kazantzidis, S., Escala, A., & Callegari, S. 2010, *Nature*, 466, 1082, doi: [10.1038/nature09294](https://doi.org/10.1038/nature09294)

Mehta, D., Regan, J. A., & Prole, L. 2024, *The Open Journal of Astrophysics*, 7, doi: [10.33232/001c.126629](https://doi.org/10.33232/001c.126629)

Mehta, D. H., Regan, J. A., & Prole, L. 2026, *Nature Astronomy*, 1

Milosavljević, M., Couch, S. M., & Bromm, V. 2009, *The Astrophysical Journal*, 696, L146, doi: [10.1088/0004-637X/696/2/L146](https://doi.org/10.1088/0004-637X/696/2/L146)

Naidu, R. P., Matthee, J., Katz, H., et al. 2025, arXiv e-prints, arXiv:2503.16596, doi: [10.48550/arXiv.2503.16596](https://doi.org/10.48550/arXiv.2503.16596)

Naidu, R. P., Oesch, P. A., Brammer, G., et al. 2026, *The Open Journal of Astrophysics*, 9, doi: [10.33232/001c.156033](https://doi.org/10.33232/001c.156033)

Nandal, D., Regan, J. A., Woods, T. E., et al. 2023, *Astronomy & Astrophysics*, 677, A155, doi: [10.1051/0004-6361/202346938](https://doi.org/10.1051/0004-6361/202346938)

Ortiz, O. A. C., Finkelstein, S. L., Plat, A., et al. 2025, Significant Evidence of an AGN Contribution in GHZ2 at $z = 12.34$, arXiv, doi: [10.48550/arXiv.2511.03035](https://doi.org/10.48550/arXiv.2511.03035)

Pacucci, F., & Loeb, A. 2024, *The Astrophysical Journal*, 964, 154, doi: [10.3847/1538-4357/ad3044](https://doi.org/10.3847/1538-4357/ad3044)

Pacucci, F., Nguyen, B., Carniani, S., Maiolino, R., & Fan, X. 2023, *The Astrophysical Journal Letters*, 957, L3, doi: [10.3847/2041-8213/ad0158](https://doi.org/10.3847/2041-8213/ad0158)

Pakmor, R., Springel, V., Bauer, A., et al. 2016, *Monthly Notices of the Royal Astronomical Society*, 455, 1134, doi: [10.1093/mnras/stv2380](https://doi.org/10.1093/mnras/stv2380)

Pakmor, R., Springel, V., Coles, J. P., et al. 2023, *Monthly Notices of the Royal Astronomical Society*, 524, 2539, doi: [10.1093/mnras/stac3620](https://doi.org/10.1093/mnras/stac3620)

Portegies Zwart, S. F., Baumgardt, H., Hut, P., Makino, J., & McMillan, S. L. W. 2004, *Nature*, 428, 724, doi: [10.1038/nature02448](https://doi.org/10.1038/nature02448)

Prole, L. R., Clark, P. C., Klessen, R. S., & Glover, S. C. O. 2022, *Monthly Notices of the Royal Astronomical Society*, 510, 4019, doi: [10.1093/mnras/stab3697](https://doi.org/10.1093/mnras/stab3697)

Prole, L. R., Regan, J. A., Glover, S. C. O., et al. 2024a, *Astronomy & Astrophysics*, 685, A31, doi: [10.1051/0004-6361/202348903](https://doi.org/10.1051/0004-6361/202348903)

Prole, L. R., Regan, J. A., Mehta, D., Coles, P., & Dayal, P. 2025, *The Open Journal of Astrophysics*, 8, doi: [10.33232/001c.143643](https://doi.org/10.33232/001c.143643)

Prole, L. R., Regan, J. A., Whalen, D. J., Glover, S. C. O., & Klessen, R. S. 2024b, *Astronomy & Astrophysics*, 692, A213, doi: [10.1051/0004-6361/202452486](https://doi.org/10.1051/0004-6361/202452486)

Prole, L. R., Regan, J. A., Mehta, D., et al. 2025, arXiv e-prints, arXiv:2511.09640, doi: [10.48550/arXiv.2511.09640](https://doi.org/10.48550/arXiv.2511.09640)

Rantala, A., & Naab, T. 2025, *Monthly Notices of the Royal Astronomical Society: Letters*, 542, L78, doi: [10.1093/mnrasl/slaf064](https://doi.org/10.1093/mnrasl/slaf064)

Regan, J., & Volonteri, M. 2024, *The Open Journal of Astrophysics*, 7, doi: [10.33232/001c.123239](https://doi.org/10.33232/001c.123239)

Regan, J. A., & Downes, T. P. 2018, *Monthly Notices of the Royal Astronomical Society*, 475, 4636, doi: [10.1093/mnras/sty134](https://doi.org/10.1093/mnras/sty134)

Regan, J. A., & Haehnelt, M. G. 2009, *Monthly Notices of the Royal Astronomical Society*, 396, 343, doi: [10.1111/j.1365-2966.2009.14579.x](https://doi.org/10.1111/j.1365-2966.2009.14579.x)

Regan, J. A., Johansson, P. H., & Wise, J. H. 2014, *The Astrophysical Journal*, 795, 137, doi: [10.1088/0004-637X/795/2/137](https://doi.org/10.1088/0004-637X/795/2/137)

Regan, J. A., Visbal, E., Wise, J. H., et al. 2017, *Nature Astronomy*, 1, 1, doi: [10.1038/s41550-017-0075](https://doi.org/10.1038/s41550-017-0075)

Regan, J. A., Wise, J. H., Woods, T. E., et al. 2020, *The Open Journal of Astrophysics*, 3, 10.21105/astro.2008.08090, doi: [10.21105/astro.2008.08090](https://doi.org/10.21105/astro.2008.08090)

Reines, A. E., & Volonteri, M. 2015, *The Astrophysical Journal*, 813, 82, doi: [10.1088/0004-637X/813/2/82](https://doi.org/10.1088/0004-637X/813/2/82)

Reinoso, B., Klessen, R. S., Schleicher, D., Glover, S. C. O., & Solar, P. 2023, Monthly Notices of the Royal Astronomical Society, 521, 3553, doi: [10.1093/mnras/stad790](https://doi.org/10.1093/mnras/stad790)

Reinoso, B., Schleicher, D. R. G., Fellhauer, M., Klessen, R. S., & Boekholt, T. C. N. 2018, Astronomy & Astrophysics, 614, A14, doi: [10.1051/0004-6361/201732224](https://doi.org/10.1051/0004-6361/201732224)

Rusakov, V., Watson, D., Nikopoulos, G., et al. 2025, arXiv preprint arXiv:2503.16595

—. 2026, Nature, 649, 574

Shi, Y., Kremer, K., Grudić, M. Y., Gerling-Dunsmore, H. J., & Hopkins, P. F. 2023, Monthly Notices of the Royal Astronomical Society, 518, 3606, doi: [10.1093/mnras/stac3245](https://doi.org/10.1093/mnras/stac3245)

Shi, Y., Kremer, K., & Hopkins, P. F. 2024, Astronomy & Astrophysics, 691, A24, doi: [10.1051/0004-6361/202450964](https://doi.org/10.1051/0004-6361/202450964)

Smith, B. D., Regan, J. A., Downes, T. P., et al. 2018, Monthly Notices of the Royal Astronomical Society, 480, 3762, doi: [10.1093/mnras/sty2103](https://doi.org/10.1093/mnras/sty2103)

Sneppen, A., Watson, D., Matthews, J. H., et al. 2026, arXiv e-prints, arXiv:2601.18864, doi: [10.48550/arXiv.2601.18864](https://doi.org/10.48550/arXiv.2601.18864)

Springel, V. 2010, Monthly Notices of the Royal Astronomical Society, 401, 791, doi: [10.1111/j.1365-2966.2009.15715.x](https://doi.org/10.1111/j.1365-2966.2009.15715.x)

Springel, V., Pakmor, R., Zier, O., & Reinecke, M. 2021, Monthly Notices of the Royal Astronomical Society, 506, 2871, doi: [10.1093/mnras/stab1855](https://doi.org/10.1093/mnras/stab1855)

Sun, W. Q., Naidu, R. P., Matthee, J., et al. 2026, arXiv preprint arXiv:2601.20929

Taylor, A. J., Kokorev, V., Kocevski, D. D., et al. 2025, CAPERS-LRD-z9: A Gas Enshrouded Little Red Dot Hosting a Broad-line AGN at $Z=9.288$, arXiv, doi: [10.48550/arXiv.2505.04609](https://doi.org/10.48550/arXiv.2505.04609)

Tremmel, M., Governato, F., Volonteri, M., & Quinn, T. R. 2015, Monthly Notices of the Royal Astronomical Society, 451, 1868, doi: [10.1093/mnras/stv1060](https://doi.org/10.1093/mnras/stv1060)

Umeda, H., Hosokawa, T., Omukai, K., & Yoshida, N. 2016, The Astrophysical Journal Letters, 830, L34, doi: [10.3847/2041-8205/830/2/L34](https://doi.org/10.3847/2041-8205/830/2/L34)

Visbal, E., Haiman, Z., & Bryan, G. L. 2014a, Monthly Notices of the Royal Astronomical Society, 445, 1056, doi: [10.1093/mnras/stu1794](https://doi.org/10.1093/mnras/stu1794)

Visbal, E., Haiman, Z., Terrazas, B., Bryan, G. L., & Barkana, R. 2014b, Monthly Notices of the Royal Astronomical Society, 445, 107, doi: [10.1093/mnras/stu1710](https://doi.org/10.1093/mnras/stu1710)

Wise, J. H., Regan, J. A., O’Shea, B. W., et al. 2019, Nature, 566, 85, doi: [10.1038/s41586-019-0873-4](https://doi.org/10.1038/s41586-019-0873-4)

Wise, J. H., Turk, M. J., & Abel, T. 2008, The Astrophysical Journal, 682, 745, doi: [10.1086/588209](https://doi.org/10.1086/588209)

Woods, T. E., Heger, A., Whalen, D. J., Haemmerlé, L., & Klessen, R. S. 2017, The Astrophysical Journal Letters, 842, L6, doi: [10.3847/2041-8213/aa7412](https://doi.org/10.3847/2041-8213/aa7412)

Zana, T., Capelo, P. R., Boresta, M., et al. 2025, Super-Eddington Accretion in Protogalactic Cores, arXiv, doi: [10.48550/arXiv.2508.21114](https://doi.org/10.48550/arXiv.2508.21114)

Zhang, S., Liu, B., Bromm, V., et al. 2025, How Do Massive Primordial Black Holes Impact the Formation of the First Stars and Galaxies?, arXiv, doi: [10.48550/arXiv.2503.17585](https://doi.org/10.48550/arXiv.2503.17585)

Ziparo, F., Gallerani, S., & Ferrara, A. 2025, Journal of Cosmology and Astroparticle Physics, 2025, 040, doi: [10.1088/1475-7516/2025/04/040](https://doi.org/10.1088/1475-7516/2025/04/040)

APPENDIX

MORE EXAMPLES OF BH FEEDBACK

Here we include more examples of plots presented within the main body of the paper, to strengthen the arguments made throughout the text.

Firstly, we show similar density and temperature projections to Figure 5 in Figures A.10 and A.11, which correspond to the host halos of N2BH2 and N2BH4, respectively. These 3 systems were chosen because they contain the only MBHs from the sample of 15 largest BHs inspected to experience no SNe explosions between the time of their creation and the eventual accretion cut-off. Therefore, the feedback effects can only be attributed to BH accretion feedback. In all cases, feedback from the MBH heats the gas to 10^7 K, expanding it beyond the virial radius of the halo, out to scales of 10 kpc.

In the main text, we presented the gas properties within the accretion sphere of N2BH1 and the estimated feedback energies in Figure 7, because it had the most snapshot outputs between the BH’s creation and its accretion cut-off. Here we present similar plots for N2BH2 and N2BH3 in Figure A.12, as these have the next highest number of snapshots during the accretion period. In all 3 cases, the accretion cut-offs occur approximately 15 Myr after the injected energy per 10^5 Myr timestep exceeds the binding energy of the halo.

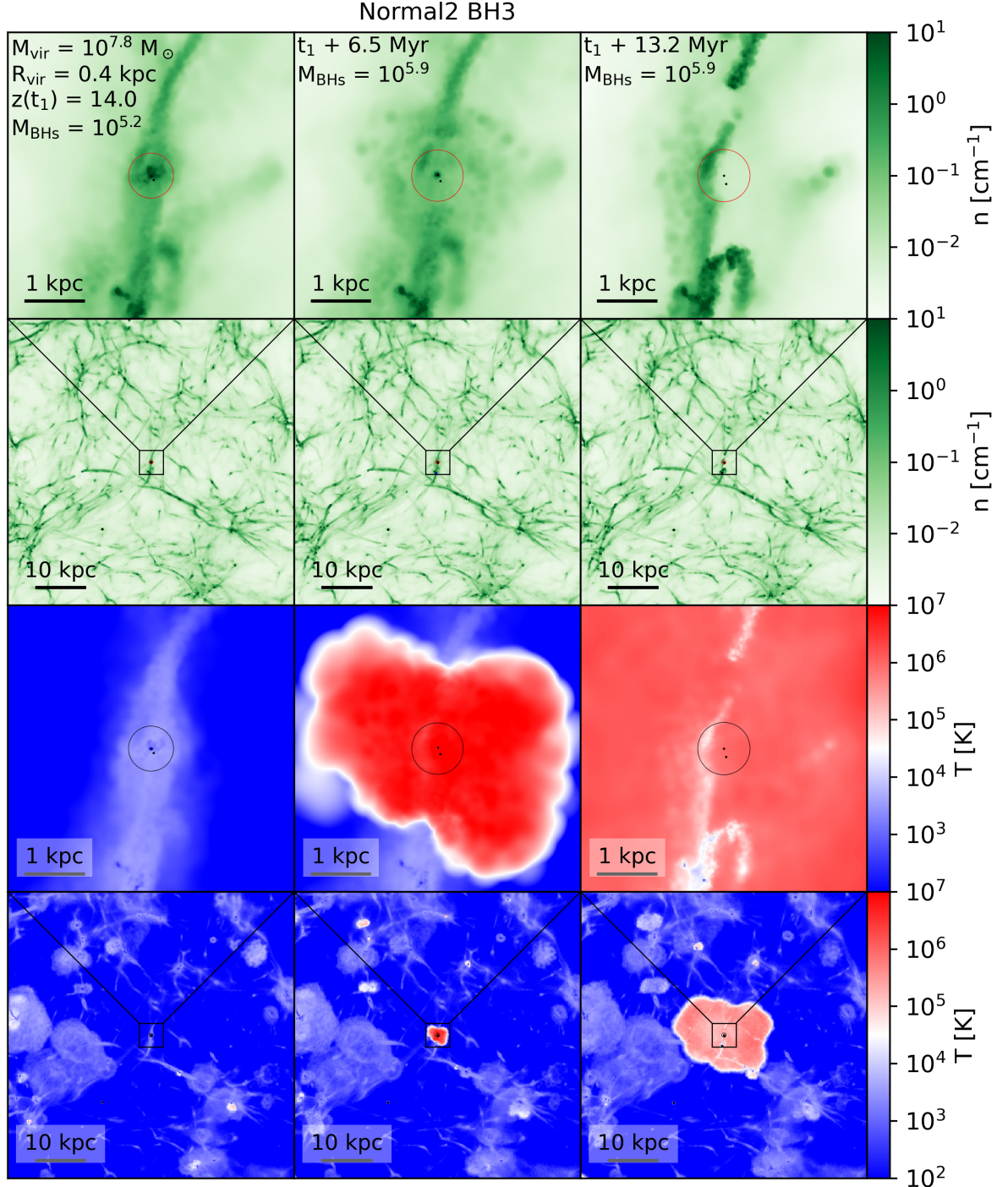


FIG. A.10.— Projections of the halo containing N2BH3 before (left), during (center) and after (right) the accretion cut-off. The top 2 panels show density projections, while the bottom 2 panels show temperature projections. In each case, the upper panel shows a region of 5 kpc, while the lower panel shows a zoom-out of 60 kpc. BHs, PopIII stars and PopII stellar cluster particles are shown as black, blue and orange dots, respectively. We show the virial radius of the halo as a circle. We include values for the virial mass, virial radius, redshift and black hole mass.

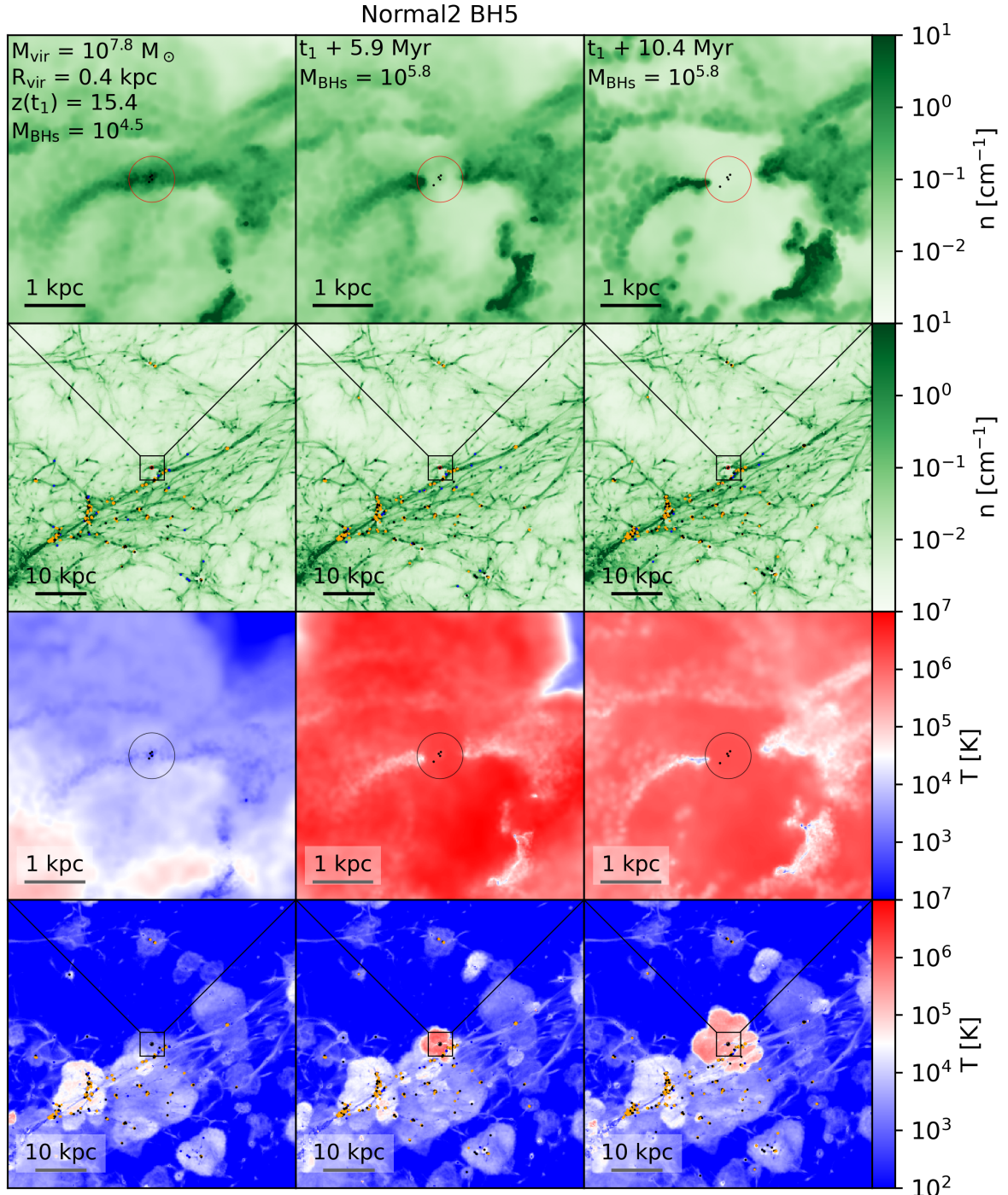


FIG. A.11.— Projections of the halo containing N2BH5 before (left), during (center) and after (right) the accretion cut-off. The top 2 panels show density projections, while the bottom 2 panels show temperature projections. In each case, the upper panel shows a region of 5 kpc, while the lower panel shows a zoom-out of 60 kpc. BHs, PopIII stars and PopII stellar cluster particles are shown as black, blue and orange dots, respectively. We show the virial radius of the halo as a circle. We include values for the virial mass, virial radius, redshift and black hole mass.

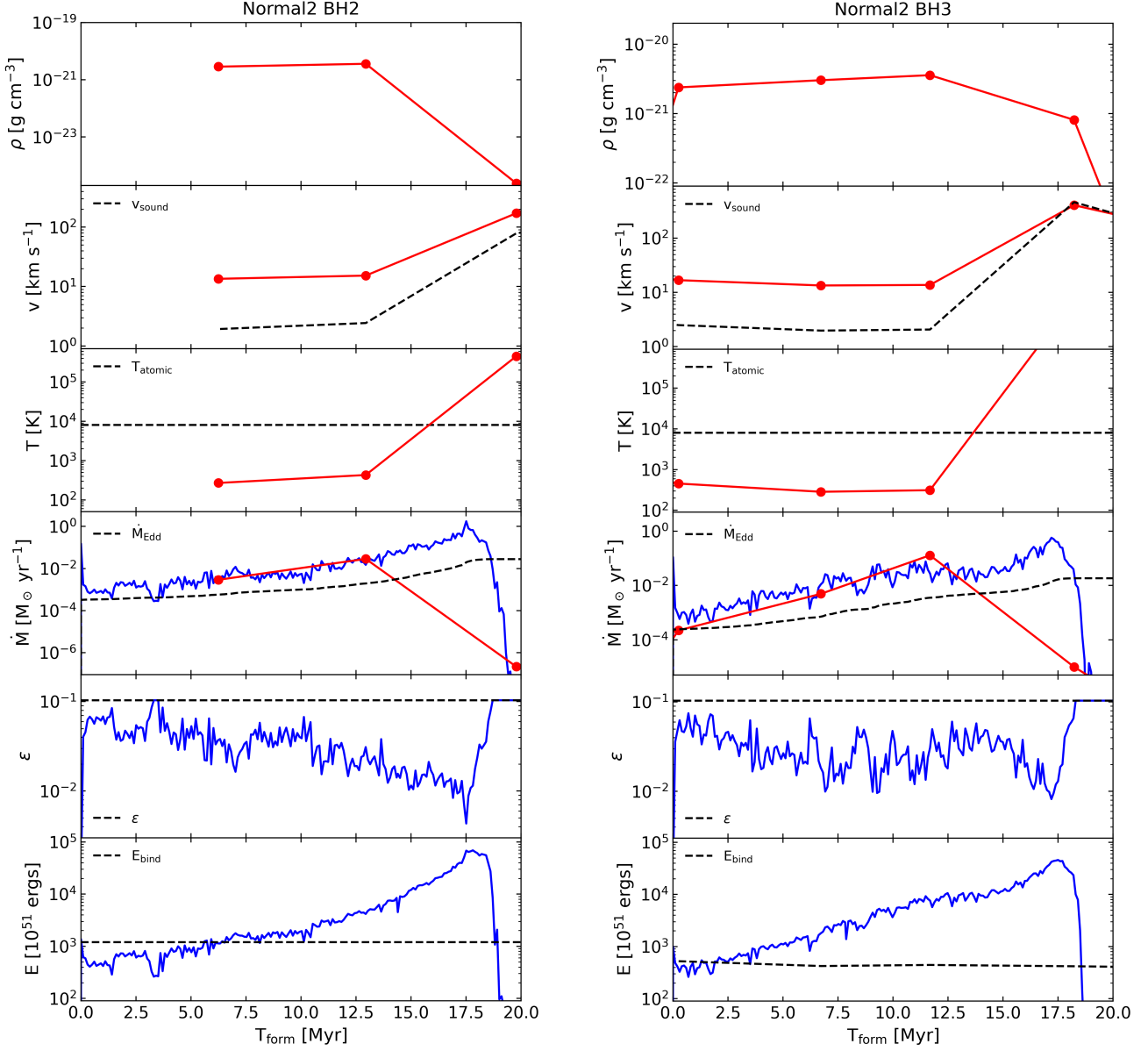


FIG. A.12.— Accretion and feedback properties of N2BH2 and N2BH3. The top 3 panels show mass weighted average density, relative velocity and temperature of the gas within the accretion sphere surrounding the BH. The sound speed is shown as a dashed line. The 4th panel shows the accretion rate onto the BH (blue) and the rate estimated from the properties in the top 3 panels (red). The 5th panel show the feedback parameter ϵ during the super-Eddington burst (blue), compared to the sub-Eddington value (dashed black). The bottom panel shows the energy injected in each timebin of roughly 10^5 yr (blue) compared to the binding energy of the halo (dashed black).